H1prelim-11-034
ZEUS-prel-11-001
Preliminary Document May 1, 2011

QCD analysis and determination of α_s using the combined H1 and ZEUS inclusive cross sections together with the jet production cross section measured by the H1 and the ZEUS experiments.

H1 and ZEUS Collaborations

Abstract

An NLO QCD PDF fit analysis with simultaneous determination of the strong coupling constant $\alpha_s(M_Z)$ is presented. The analysis is based on the same combined H1 and ZEUS inclusive DIS measurements as the HERAPDF1.5 fit, together with jet measurements provided by both the H1 and ZEUS collaborations. The inclusion of jet data in the analysis significantly reduces the correlation between the gluon parton density function and the strong coupling constant, improving the precision of the gluon PDF and providing an accurate unbiased determination of $\alpha_s(M_Z)$.

1 Introduction

The analysis presents the PDF QCD analysis with the simultaneous determination of the strong coupling constant $\alpha_s(M_Z)$. The large correlation between the gluon density function and the strong coupling constant, leading to a high experimental uncertainty on both the gluon PDF and α_s, has been significantly reduced by the inclusion of the H1 and ZEUS jet data to the fit.

1.1 Data used in the PDF fit

The cross sections of jet production in DIS as measured by the H1 [4, 5] and ZEUS [6, 7] experiments are used in the analysis together with the combined NC and CC cross sections from the HERA I [1] and HERA II running periods [2].

To study the impact of the jet measurements on the simultaneous determination of the gluon density function and the strong coupling constant, the following jet data sets are used:

- H1 HERA I+II high Q^2 DIS normalized inclusive jet data [4]
  The measurement in the kinematic range of $150 < Q^2 < 15000$ GeV^2 is based on the data collected in the HERAI and HERAII running periods and correspond to an integrated luminosity of 395 pb^{-1}. In this study only the normalized inclusive jet cross section measurement as a function of P_T and Q^2 is used (see table 4 in [4]).

- H1 HERA I low Q^2 DIS inclusive jet data [5]
  The measurement has been performed in the kinematic range of $5 < Q^2 < 100$ GeV^2 and is based on the data colleced in the HERA I running period, corresponding to an integrated luminosity of 43.5 pb^{-1}. This measurement has particularly large theoretical uncertainties due to missing orders of the pQCD calculation. In this study only the inclusive cross section points as a function of Q^2 and P_T were used. The data points with large k-factors (NLO to LO ratio) of > 2.5 have been excluded.

- ZEUS HERA I 96/97 high Q^2 DIS inclusive jet data [6]
  The measurement is performed in the kinematic range of $Q^2 > 125$ GeV^2 and based on the data collected in the 1996-1997 HERA running period, corresponding to an integrated luminosity of 38.6 pb^{-1}.

- ZEUS HERA I 98-00 high Q^2 DIS inclusive jet data [7]
  The measurement is performed in the same kinematic range as [6] but is based on the data collected in 1998-2000, corresponding to an integrated luminosity of 82 pb^{-1}.

  The fit uing only inclusive DIS data in the following is referred to as HERAPDF1.5. If the four mentioned above jet data sets are used simultaneously with the inclusive DIS data it is called HERAPDF1.6 fit.

1.2 Parametrisation

The PDF fit is performed using NLO DGLAP equations, for which the evolution code QCDNUM 17 [10] is used. Heavy quarks are treated as massive using the RT variable flavour number scheme [11, 12].

Two parametrisations are studied: a 10-parameter fit which corresponds to the preliminary PDF fit of the NC and CC combined HERA I and HERA II data, HERAPDF1.5 [3], and a 14-parameter fit, HERAPDF1.5f, which allows more flexibility, in particular for the low-x gluon distribution. At the starting scale $Q_0^2 = 1.9$ GeV^2 the PDFs are parametrized as follows:

$$
\begin{aligned}
xg(x) &= A_g x^{B_g} \cdot (1-x)^{C_g} - A'_g x^{B'_g} (1-x)^{C'_g} && (1)\\
xu_v(x) &= A_{u_v} x^{B_{u_v}} \cdot (1-x)^{C_{u_v}} \cdot (1 + D_{u_v} x + E_{u_v} x^2) && (2)\\
xd_v(x) &= A_{d_v} x^{B_{d_v}} \cdot (1-x)^{C_{d_v}} && (3)\\
x\bar{U}(x) &= A_{\bar{U}} x^{B_{\bar{U}}} \cdot (1-x)^{C_{\bar{U}}} && (4)\\
x\bar{D}(x) &= A_{\bar{D}} x^{B_{\bar{D}}} \cdot (1-x)^{C_{\bar{D}}} && (5)
\end{aligned}
$$

The parameters A_g, A_{u_v}, A_{d_v} are constrained by the sum rules. It is assumed that $B_{\bar{U}} = B_{\bar{D}}$, $C'_g = 25$, $A_{\bar{U}} = A_{\bar{D}}(1 - f_s)$, where f_s is the strangeness fraction.

In the 10-parameter fit additional four constraints are enforced: $A'_g = B'_g = 0$, $B_{d_v} = B_{u_v}$ and $D_{u_v} = 0$. In both, the 10- and 14-parameter fits these choices define the central fit, while further parameters are considered when evaluating the parametrization uncertainty, as described in section 2.3.

Greater flexibility in the gluon density helps to avoid a parametrisation bias, when adding more data that is sensitive to the gluon density, like charm or jet production. Therefore, the 14-parameter fit is preferred and used for HERAPDF1.6.

1.3 Theoretical predictions

The NLO cross sections of jet production were calculated using the NLOJET++ program [13]. The FastNLO [14] interface was used to efficiently convolute the matrix elements from NLOJET++ with the fitted PDFs.

In the prediction for the normalized jet cross sections [4] QCDNUM has been used to calculate the corresponding inclusive cross sections. For the factorisation and renormalisation scales the same variables as in relevant publications are used, the combination of Q^2 and transverse jet energy measured in the Breit frame E_T ($\mu_f = \mu_r = \sqrt{(Q^2 + E_T^2)/2}$) for the H1 measurements and transverse jet energy measured in the Breit frame ($\mu_f = \mu_r = \sqrt{E_T^2}$) for the ZEUS measurements.

2 Determination of uncertainties

The total uncertainty of the parton density functions and the $\alpha_s$accounts for the experimenal uncertainties of the measurements and the variations of model and parametrisation assumptions, as described in the following.

2.1 Experimental uncertainty

The experimental uncertainties of the H1 and ZEUS combined NC and CC cross sections are accounted for following the description in [1]. The details on the determination of the experimental uncertainties of the jet cross sections are described in [4, 5, 6, 7]. Twelve systematic error sources are treated as correlated between data points of a given measurement and as uncorrelated between different measurements. In addition a theoretical uncertainty on the luminosity measurement of 0.5% has been considered as correlated between all H1 and ZEUS jet measurements. The considered correlated error sources are summarized in Table 1.

Source of correlated uncertainty	**Correlation fraction**	**Data set**
H1 LAr electron energy scale (99-07)	25%	[4]
H1 LAr electron angle (99-07)	100%	[4]
H1 Jet energy scale (99-07)	50%	[4]
H1 Luminosity (99-00)	100%	[5]
H1 Spacal electron energy scale (99-00)	50%	[5]
H1 Spacal electron angle (99-00)	50%	[5]
H1 Jet energy scale (99-00)	50%	[5]
H1 low Q^2 jet measurement model dependence	50%	[5]
ZEUS luminosity measurement (96-97)	100%	[6]
ZEUS jet energy scale (96-97)	100%	[6]
ZEUS luminosity measurement (98-00)	100%	[7]
ZEUS jet energy scale (98-00)	100%	[7]
Theoretical luminosity measurement uncertainty	100%	[4], [5], [6], [7]

Table 1: Experimental uncertainties and the correlation fraction for the particular jet data set.

2.2 Model uncertainty

The model assumption variations are the same to those performed for HERAPDF1.0 [1]. They are summarized in table 2.

Model parameter	**Standard value**	**Lower Limit**	**Upper Limit**
Strange fraction f_s	0.31	0.23	0.38
Charm mass m_c [GeV]	1.4	1.35	1.65
Beauty mass m_b [GeV]	4.75	4.3	5.0
Minimum Q^2 [GeV^2]	3.5	2.5	5.0

Table 2: Assumed parameters of the model and their variations.

In addition the hadronization uncertainty for each of the jet data samples is taken into account. All the model uncertainties are added in quadrature.

The renormalisation and factorization scales are varied separately for the jet NLO cross section predictions but simultaneously for all the data sets. This variation corresponds to $1/2\mu < \mu_{f,r} < 2\mu$.

2.3 Parametrisation uncertainty

For the parametrization uncertainty estimation the generalized parametrization is studied:

$$xg(x,Q_0^2) = Ax^B \cdot (1-x)^C \cdot (1 - Dx + Ex^2 + \epsilon\sqrt{x}) - A'x^{B'} \cdot (1-x)^{C'} \quad (6)$$

$$xf(x,Q_0^2) = Ax^B \cdot (1-x)^C \cdot (1 - Dx + Ex^2 + \epsilon\sqrt{x}) \quad (7)$$

where f refers to $u_v, d_v, \bar{U}, \bar{D}$.

For the HERAPDF1.5 parametrization the negative gluon term is neglected ($A' = B' = C' = 0$). All the other additional parameters are added one at a time resulting in a set of 11 free parameter fits. Further two parametrizations, one with $B_{\bar{U}} = B_{\bar{D}}$, the other with $B_{d_v} = B_{u_v}$ contrains released are also considered. Finally, the starting scale at which ditributions assume their analytic form is varied between $Q_0^2 = 1.5$ GeV^2 and $Q_0^2 = 2.5$ GeV^2. For the variation down to $Q_0^2 = 1.5$ GeV^2 the negative gluon term is enabled.

For HERAPDF1.5f and HERAPDF1.6 adding parameters one at a time results in a set of 15 free parameter fits. The starting scale has been varied in the same range as for HERAPDF1.5 and additional parametrization with $B_{\bar{U}} = B_{\bar{D}}$ constrain removed has been considered.

The most significant parametrization variation for all the fits is the variation of the starting scale. The difference between all these parametrization variations and the central fit is used to contruct an envelope representing the maximal deviation at each x value which represents the parametrization uncertainty.

3 Results

The PDF fits using the jet data are performed for the case when α_S is fixed or is a free parameter of the fit. The values of α_s, number of data points and the χ^2 for the 10 and 14-parameter fits including or not the jet data are summarized in table 3.

Fit	Nparam	DIS χ^2	jets χ^2	α_S	DIS Ndp	jets Ndp
HERAPDF1.5	10	735.9	-	fixed, 0.1176	674	-
HERAPDF1.5f	14	729.8	-	fixed, 0.1176	674	-
HERAPDF1.5 + α_s	$10 + \alpha_s$	734.7	-	free, 0.1198 ± 0.0024	674	-
HERAPDF1.5f + α_s	$14 + \alpha_s$	729.5	-	free, 0.1186 ± 0.0037	674	-
HERAPDF1.6	14	730.2	81.3	fixed, 0.1176	674	106
HERAPDF1.6 + α_s	$14 + \alpha_s$	730.0	77.6	free, 0.1202 ± 0.0013	674	106

Table 3: The χ^2 for the fits using 10 or 14 parameters. If the jet data are used, the partial χ^2 for the jet data is also indicated. The strong coupling α_s is fixed or treated as a parameter of the fit. The values of α_s obtained in the fit are given together with their experimental uncertainty.

3.1 Fits using fixed strong coupling $\alpha_s = 0.1176$

In Fig. 1 and Fig. 2 the HERAPDF1.5 and HERAPDF1.5f are shown as functions of x at photon virtuality $Q^2 = 10$ GeV^2. In both cases the strong coupling constant is fixed $\alpha_s = 0.1176$. The

total uncertainty for HERAPDF1.5 and HERAPDF1.5f is similar, but the dominant part of the parametrisation uncertainty on HERAPDF1.5 is absorbed into the experimental uncertainty for HERAPDF1.5f. This is due to larger parametrization flexibility used for HERAPDF1.5f fit. The HERAPDF1.5f yields a softer sea density at high x and a suppressed d-valence at low x as compared to HERAPDF1.5.

In Fig. 3 the summary of the PDFs is shown for the HERAPDF1.5 and HERAPDF1.5f.

In Fig. 4 the PDFs obtained using the H1 and ZEUS jet measurements is shown for a 14 parameter fit. This fit including jet data is called HERAPDF1.6. Very little difference in the size of the uncertainties for the fit using or not using the jet data is observed, however the high-x gluon PDF has a smaller uncertainty when using the jet data.

The blue lines indicate the shape of the HERAPDF1.5f fit using only inclusive data so that the shape of the PDF with and without jet data may be easily compared. The sea density gets softer at high-x when jet data are included.

In Fig. 5 the summary of the PDFs obtained using the jet data is shown.

3.2 Determination of α_s

The PDF fit was performed using the strong coupling $\alpha_s(M_Z)$ as a free parameter. As a result, with a χ^2 of 807.6 for 780 data points, the α_s was determined as

$$\alpha_S(M_Z) = 0.1202 \pm 0.0013(\text{exp}) \pm 0.0007(\text{model/param}) \pm 0.0012(\text{hadronisation}) ^{+0.0045}_{-0.0036}(\text{scale}).$$

The jet data introduces a strong sensitivity to α_s allowing a simultaneous fit with PDFs. This is illustrated in in Fig. 6, where the χ^2 for the PDF fit using α_s as a free parameter is shown as a function of the α_s value. The fit with the inclusive data alone shows a shallow minimum, while the addition of the jet data provides a severe constraint on the α_s value.

In addition to the sensitivity to α_s the jet data provides an additional constrain on the gluon density. The data reduces significantly the strong correlation between α_s and the gluon density observed when fitting the inclusive data only. In Fig. 7 the PDFs obtained in the fit using the α_s as a free parameter are shown for $Q^2 = 10$ GeV^2. If α_s is a free parameter in the fit to the inclusive data only, the gluon density has a very large uncertainty. A freedom in α_s affects only the gluon density as can be seen by comparing HERAPDF1.6 with the free α_s and HERAPDF1.6 fit with fixed α_s.

Figure 8 presents the comparison of the α_s obtained in this analysis to the world average value [9] and different H1 ([4], [5]) and ZEUS ([6], [8]). measurements. One should note that the error on the fitted α_s value due to the PDF uncertainty for the jet publications is usually included in the theoretical uncertainty, while for HERAPDF1.6 it is part of the experimental error.

In Fig. 9-Fig. 12 the measured jet cross sections used for the PDF fit HERAPDF1.6 are shown in comparison to the NLO prediction using the parton densities HERAPDF1.6 with free α_s. The ratio of data to theory is presented. The NLO prediction describes the data very well within the uncertainties. The dominant error on the prediction originates from the variation of factorisation and renormalisation scales.

3.3 Summary

The impact of jet measurements on the determination of PDFs and the strong coupling constant α_s is studied. For this purpose the jet cross section measurements by H1 and ZEUS experiments are included into the PDF fit to the combined H1 and ZEUS NC and CC cross section measurements based on the HERAI and HERAII data samples.

Two parametrisations of the PDFs are studied using the combined H1 and ZEUS NC and CC cross sections. Greater flexibility in the gluon distribution helps to avoid parametrisation bias, epecially when adding more data which is sensitive to the gluon distribution, like charm or jet production. This flexible parametrization HERAPDF1.5f is consistent with the more rigid parametrization of HERAPDF1.5, but results in a softer sea distribution at high x.

The PDF fit of the combined H1 and ZEUS NC and CC cross section measurements based on HERAI and HERAII data samples together with the jet cross section measurements from H1 and ZEUS is performed using the flexible parametrization. This fit, called HERAPDF1.6 is made with fixed and free α_s. Parton density functions resulting from the fixed α_s version of the fit are consistent with those from HERAPDF1.5f, which is based on inclusive data only, but have a softer sea distribution at high-x.

The impact of the jet data on the PDF fit using the strong coupling constant α_s as a free parameter of the fit was studied. HERAPDF1.5f, based on inclusive data, and HERAPDF1.6, in which jet data are used in addition, are compared. While HERAPDF1.5f with free α_s is not very sensitive to the α_s value, the HERAPDF1.6 fit has strong sensitivity to the value of α_s. In the HERAPDF1.6 + α_s fit the value of $\alpha_s(M_Z)$ was determined together with the parton density functions. The addition of the jet cross sections into the PDF fit reduces ignificantly the strong correlation between the gluon distribution and the strong coupling constant.

References

[1] Aaron, F. D. *et al.* [H1 and ZEUS Collaborations] 'Combined Measurement and QCD Analysis of the Inclusive ep Scattering Cross Sections at HERA', JHEP **01** (2010) 109 [arXiv:0911.0884]

[2] 'Combined Measurement of Neutral and Charged Current Cross Sections at HERA', (H1prelim-10-141, ZEUS-prel-10-017)

[3] 'PDF fits including HERA-II high Q^2 data', (H1prelim-10-142, ZEUS-prel-10-018)

[4] F. D. Aaron *et al.* [H1 Collaboration], 'Jet Production in ep Collisions at High Q^2 and Determination of α_s', Eur. Phys. J. C**65** (2010) 363-383 [arXiv:0904.3870]

[5] F. D. Aaron *et al.* [H1 Collaboration], 'Jet Production in ep Collisions at Low Q^2 and Determination of α_s', Eur. Phys. J. C**67** (2010) 1-24 [arXiv:0911.5678]

[6] S. Chekanov *et al.* [ZEUS Collaboration], 'Inclusive jet cross sections in the Breit frame in neutral current deep inelastic scattering at HERA and determination of α_s', Physics Letters B**547** (2002) 164-180 [DESY-02-112]

[7] S. Chekanov *et al.* [ZEUS Collaboration], 'Inclusive-Jet and Dijet Cross Sections in Deep Inelastic Scattering at HERA', Nuclear Physics B**765** (2007) 1-30 [DESY-06-128]

[8] S. Chekanov *et al.* [ZEUS Collaboration], 'Jet-radius dependence of inclusive-jet cross sections in deep-inelastic scattering at HERA', Physics Letters B**649** (2007) 12 [DESY-06-241]

[9] S. Bethe *et al.* [ZEUS Collaboration], Eur. Phys. J. C**64** (2009) 689

[10] M. Botje, QCDNUM version 17, http://www.nikhef.nl/∼h24/qcdnum

[11] R. S. Thorne, R. G. Roberts, 'An Ordered Analysis of Heavy Flavour Production in Deep Inelastic Scattering', Phys.Rev. **D57** (1998) 6871-6898 [hep-ph/9709442]

[12] R. S. Thorne, 'A Variable-Flavour Number Scheme for NNLO', Phys.Rev. **D73** (2006) 54019 [hep-ph/0601245]

[13] Z. Nagy and Z. Troscanyi, 'NLOJET++ 4.0.1', Phys.Rev.Lett **87** (2001) 082001 [hep-ph/0104315]

[14] T. Kluge, K. Rabberts, M. Wobisch, 'FastNLO 1.0' [hep-ph/0609285]

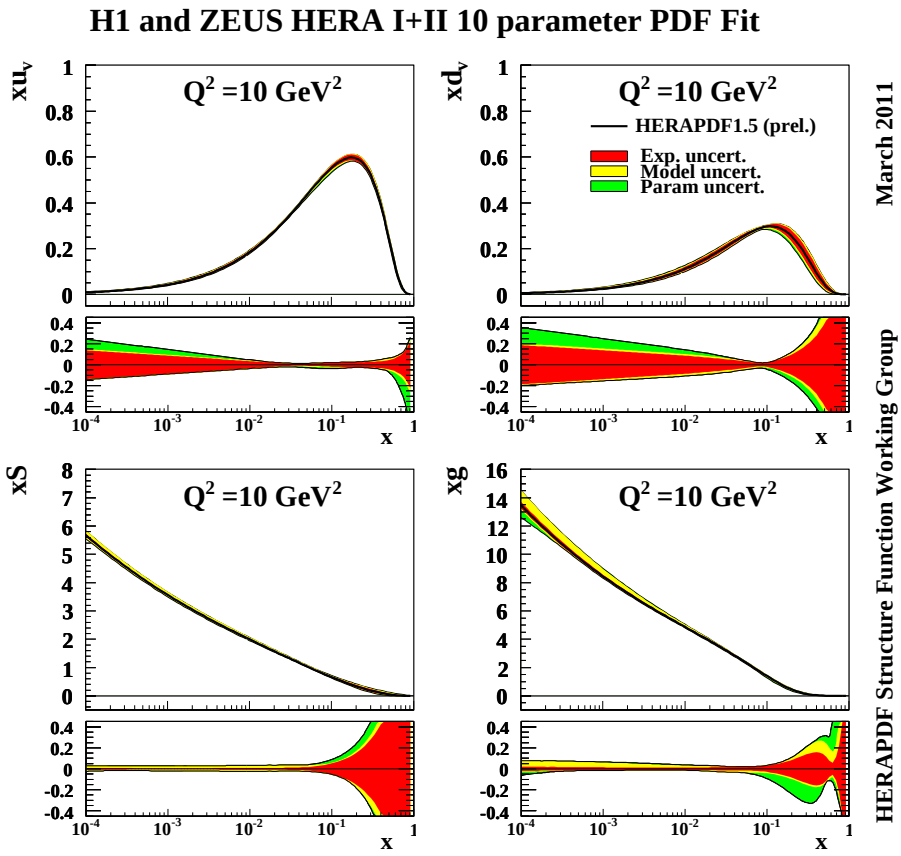

Figure 1: Valence, sea and gluon distributions for HERAPDF1.5 as a function of x for $Q^2 = 10$ GeV^2. The central value (solid line) is shown together with the experimental, model and parametrization uncertainties represented by the red, yellow and green shaded bands, respectively. The fractional uncertainties are represented separately below each of the parton densities.

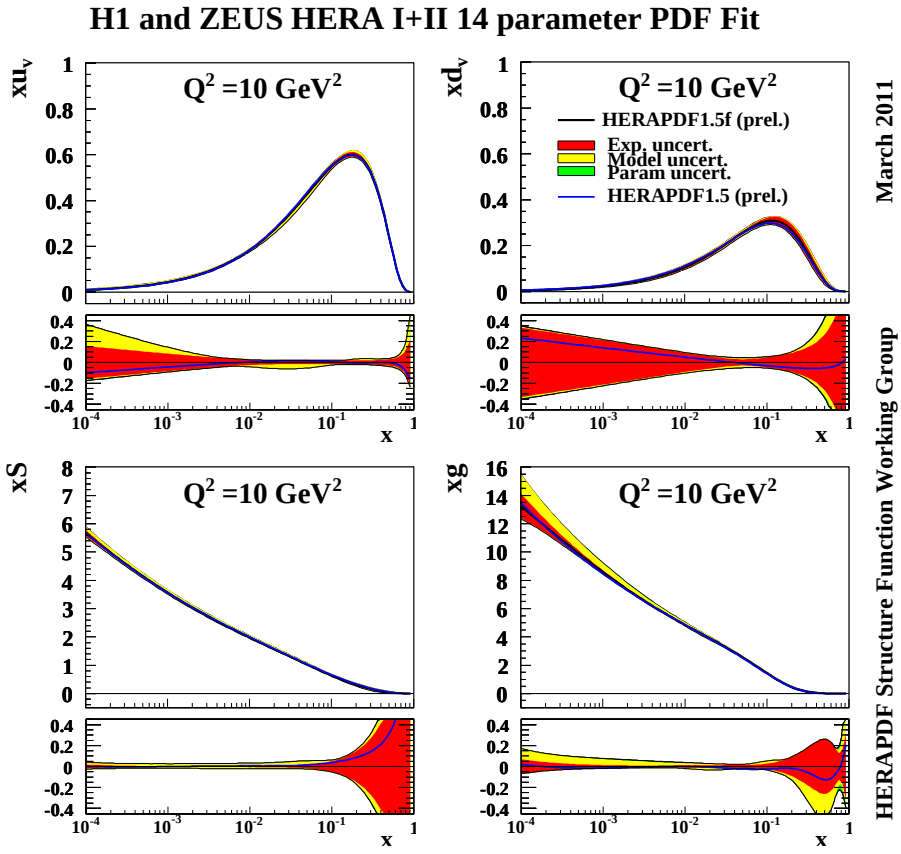

Figure 2: Valence, sea and gluon distributions for HERAPDF1.5f as a function of x for $Q^2 = 10$ GeV^2. The central value (solid line) is shown together with the experimental, model and parametrization uncertainties represented by the red, yellow and green shaded bands, respectively. Also, the central values for HERAPDF1.5 is represended by the blue line. The fractional uncertainties are represented separately below each of the parton densities together with the ratio of the central values of HERAPDF1.5 and HERAPDF1.5f (blue line).

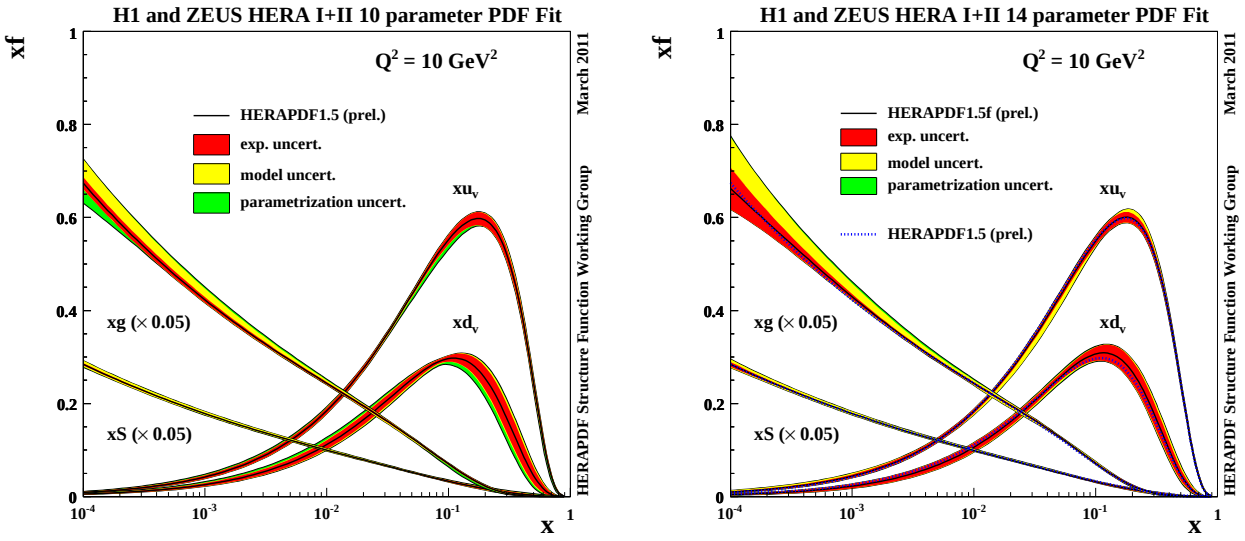

Figure 3: Parton density functions for HERAPDF1.5(left) and HERAPDF1.5f (right) as a function of x for $Q^2 = 10$ GeV^2. The central value (solid line) is shown together with the experimental, model and parametrization uncertainties represented by the red, yellow and green shaded bands, respectively.

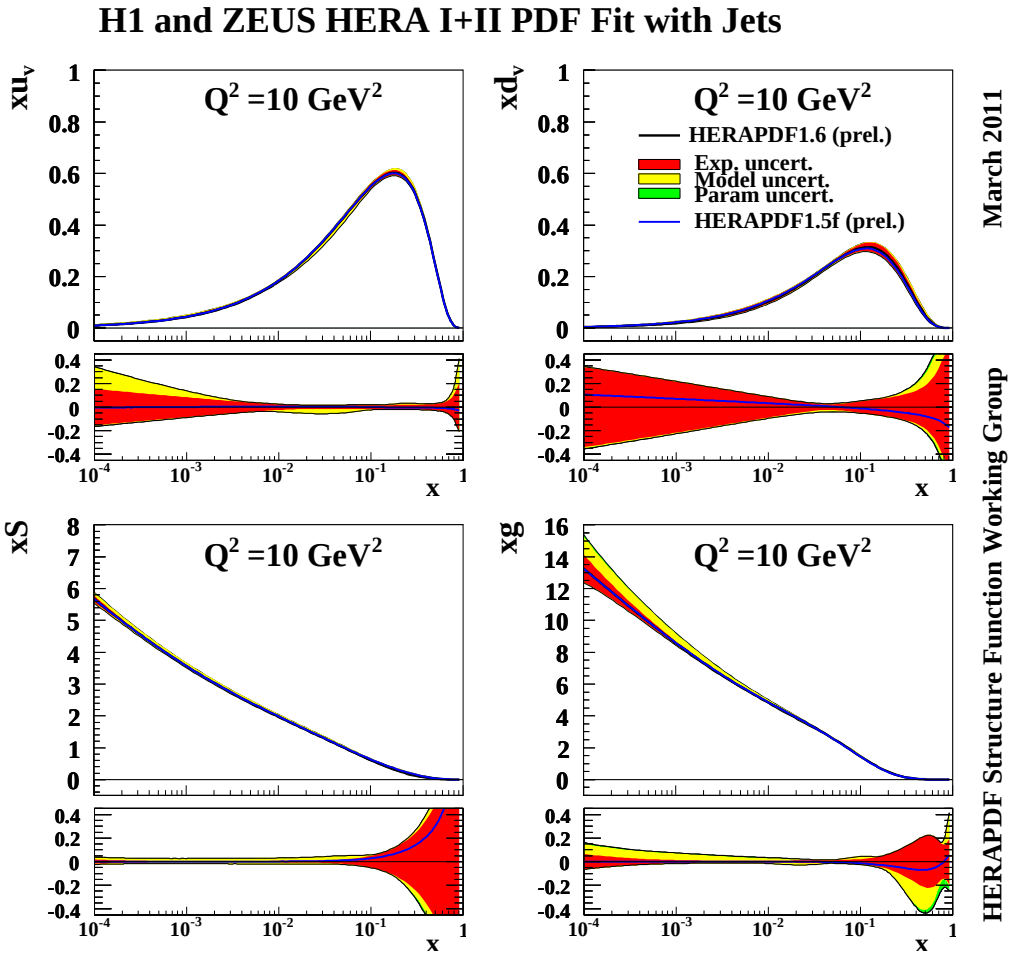

Figure 4: Valence, sea and gluon distributions for HERAPDF1.6 shown as a function of x for $Q^2 = 10$ GeV^2. The central value (solid line) is shown together with the experimental, model and parametrization uncertainties represented by the red, yellow and green shaded bands, respectively. Also, the central values for HERAPDF1.5f is represended by the blue line. The fractional uncertainties are represented separately below each of the parton densities together with the ratio of the central values of HERAPDF1.6 and HERAPDF1.5f (blue line).

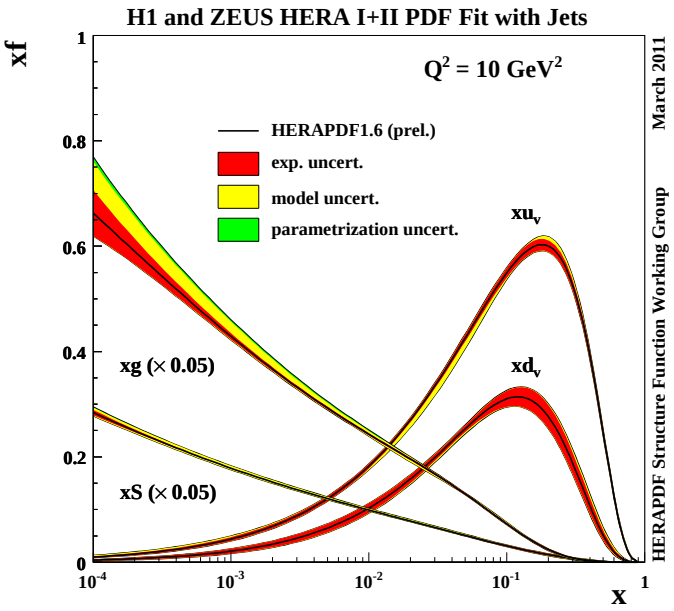

Figure 5: Parton distribution functions for HERAPDF1.6 as a function of x for $Q^2 = 10$ GeV^2. The central value (solid line) is shown together with the experimental, model and parametrization uncertainties represented by the red, yellow and green shaded bands, respectively.

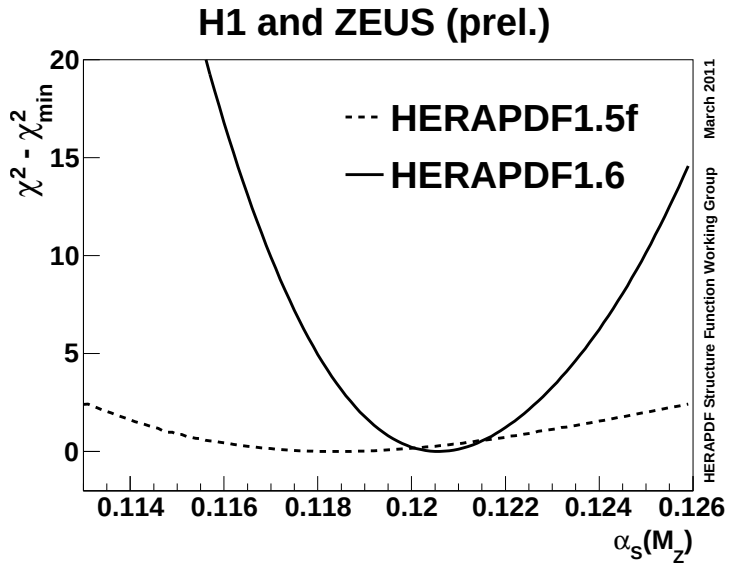

Figure 6: $\Delta\chi^2$ distribution as a function of $\alpha_s(M_Z)$ value in the PDF fits for HERAPDF1.5f (dashed line) and HERAPDF1.6 (solid line).

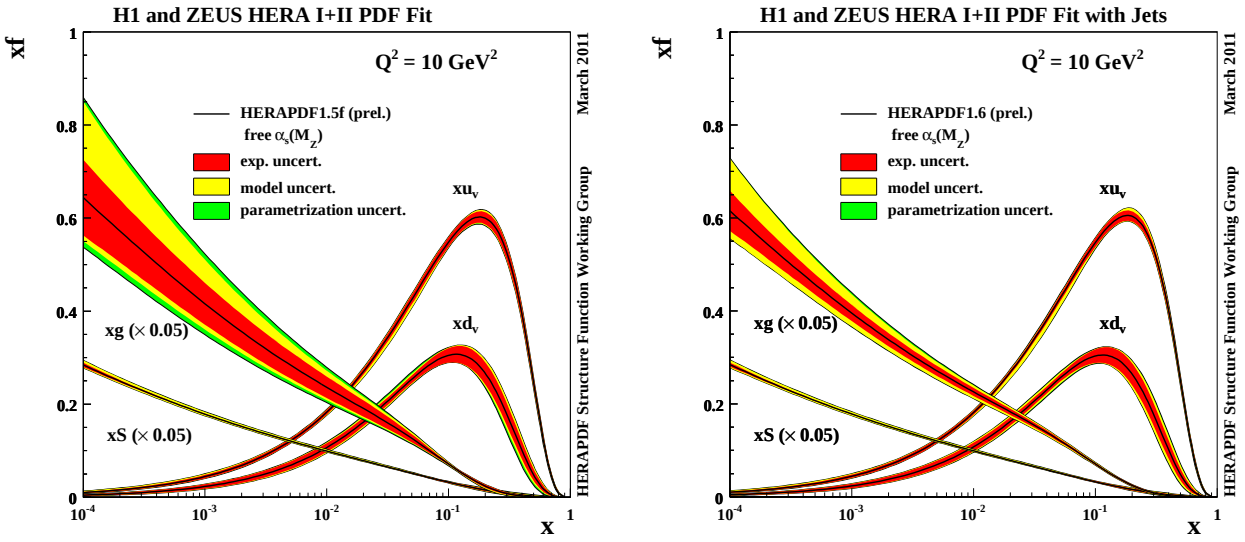

Figure 7: Parton distribution functions for HERAPDF1.5f (left) and HERAPDF1.6 (right) as a function of x for $Q^2 = 10$ GeV^2. The strong coupling constant α_s is used as a free parameter in both fits. The central values of the PDFs (solid lines) are shown together with the experimental, model and parametrization uncertainties represented by the red, yellow and green shaded bands, respectively.

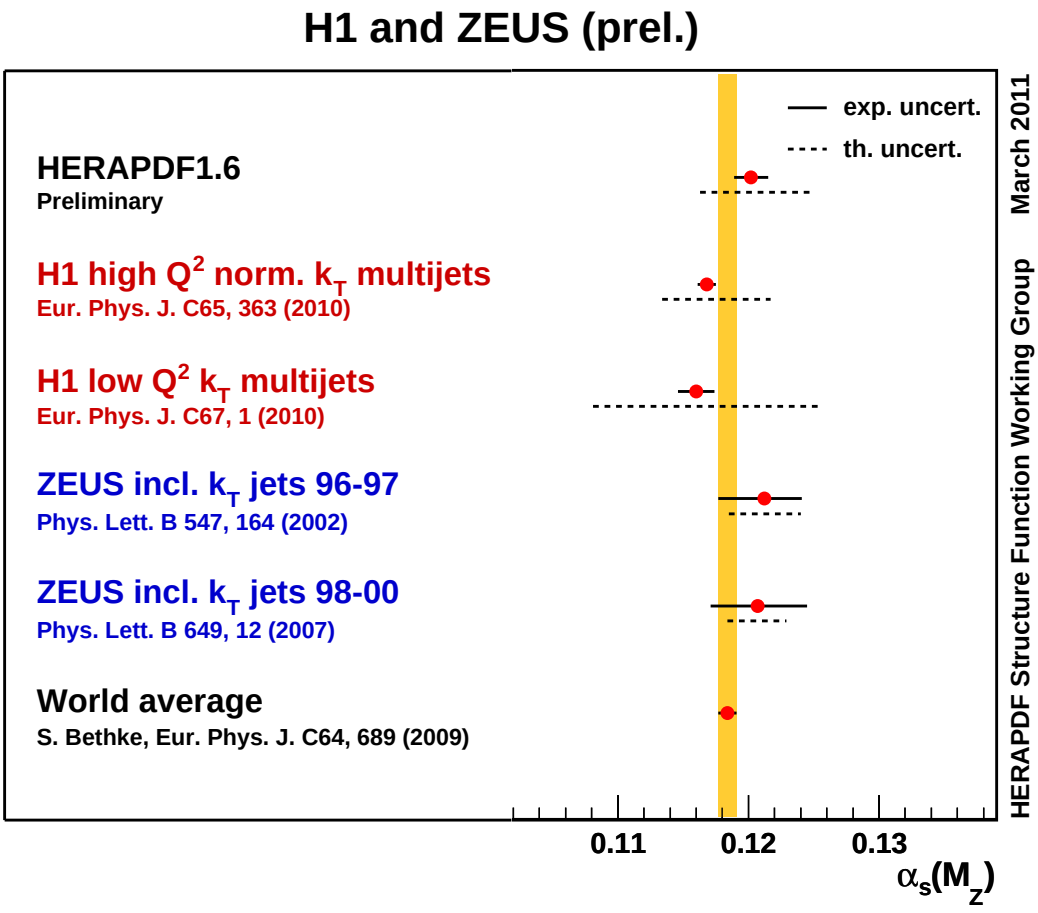

Figure 8: The fitted α_s value compared to the different H1 and ZEUS α_s measurements and the world average.

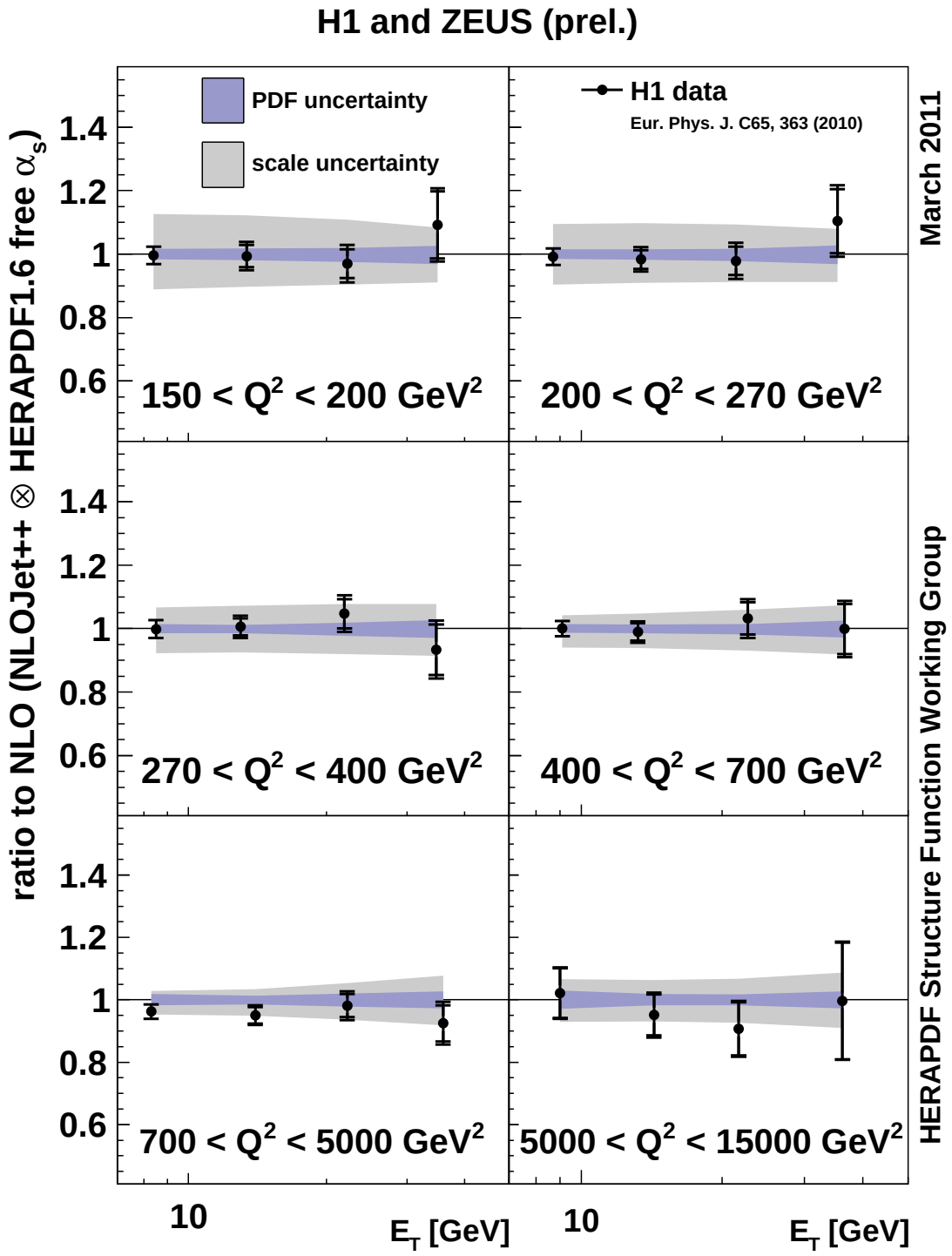

Figure 9: The ratio of the high Q^2 normalized inclusive jet data [4] used in the fit to the NLO prediction using the fitted HERAPDF1.6 PDF set and fitted $\alpha_s(M_Z) = 0.1202$. The inner error bars represent the uncorrelated errors, while the outer indicate the total error. The theoretical error band is separated into PDF error including experimental, parametrization and model uncertainties added in quadrature and the scale error depicting the uncertainty coming from the missing orders in the caluclations.

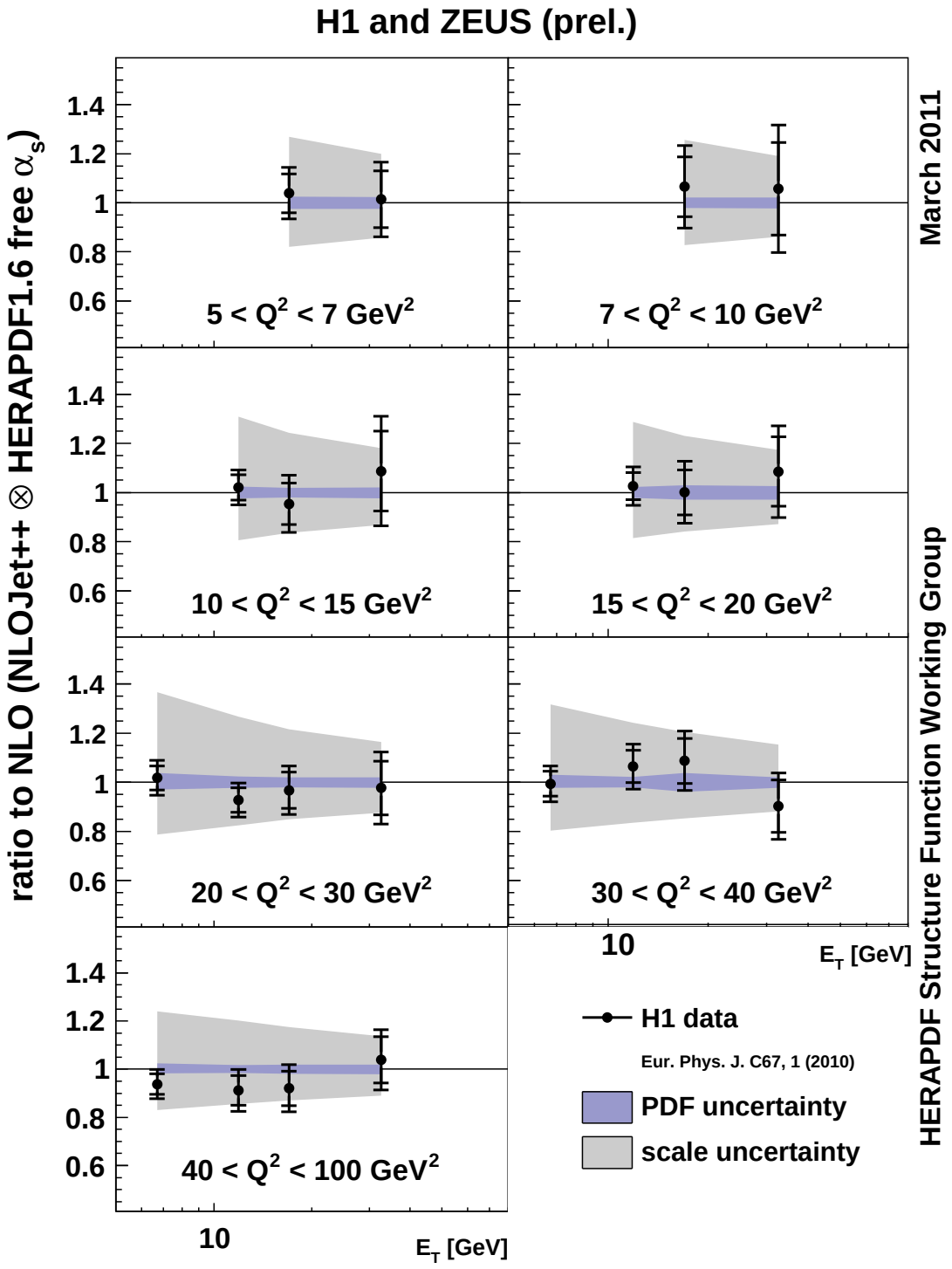

Figure 10: The ratio of the low Q^2 inclusive jet data [5] used in the fit to the NLO prediction using the fitted HERAPDF1.6 PDF set and fitted $\alpha_s(M_Z) = 0.1202$. Other details are explained in the caption of figure 9.

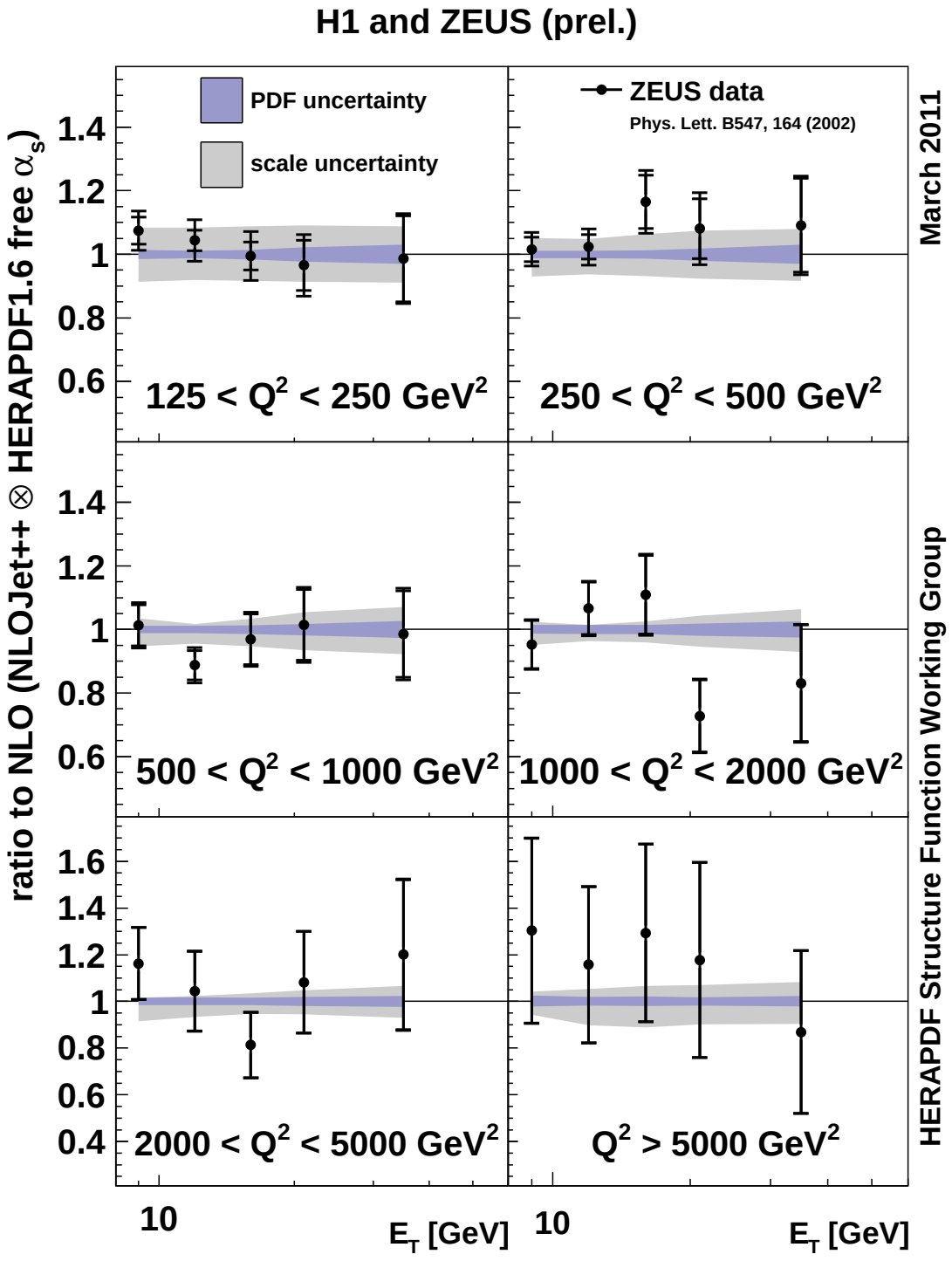

Figure 11: The ratio of the high Q^2 inclusive jet data [6] used in the fit to the NLO prediction using the fitted HERAPDF1.6 PDF set and fitted $\alpha_s(M_Z) = 0.1202$. Other details are explained in the caption of figure 9.

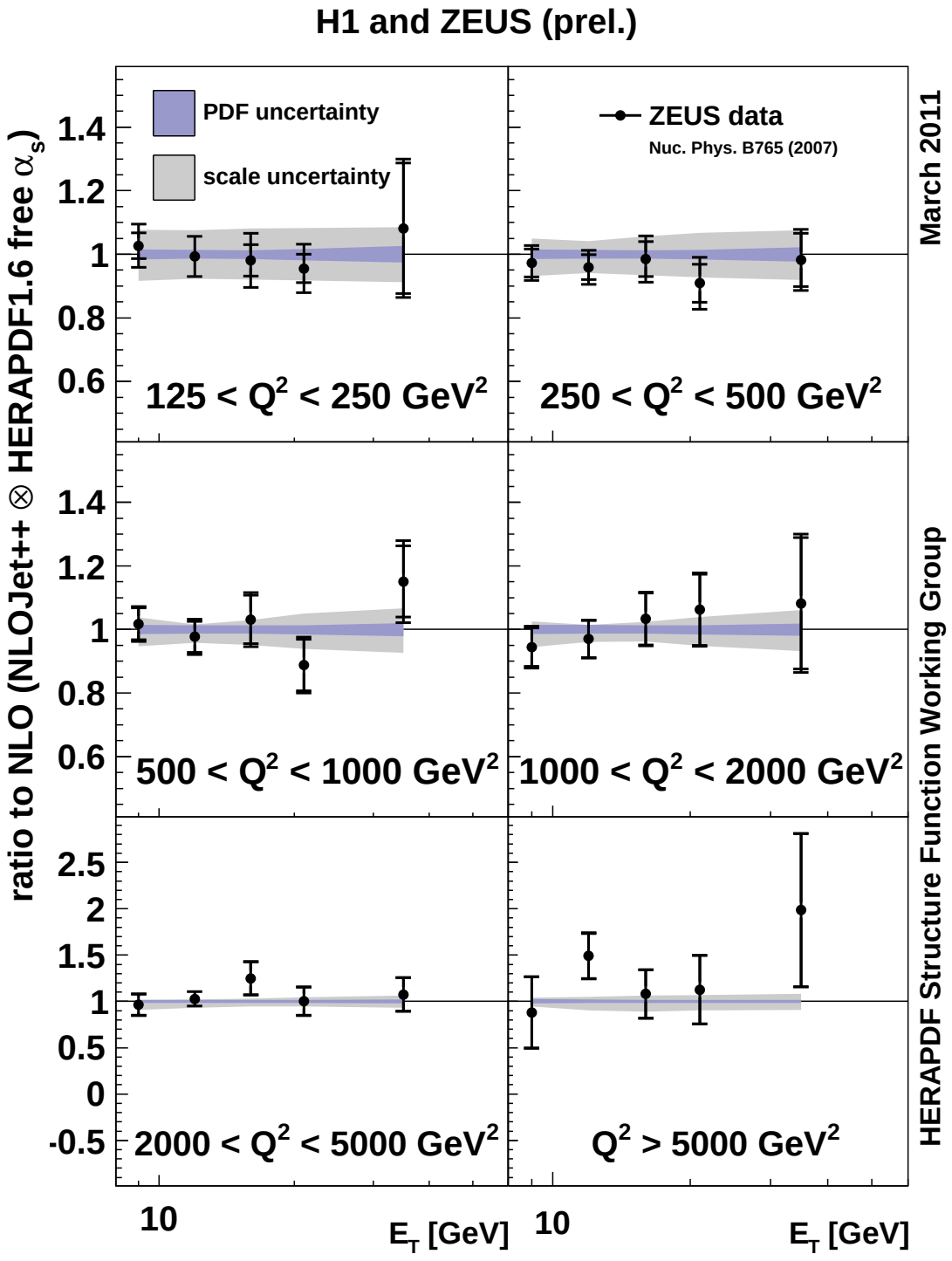

Figure 12: The ratio of the high Q^2 inclusive jet data [7] used in the fit to the NLO prediction using the fitted HERAPDF1.6 PDF set and fitted $\alpha_s(M_Z) = 0.1202$. Other details are explained in the caption of figure 9.